



CHORUS

This is the accepted manuscript made available via CHORUS. The article has been published as:

Multibeam synthesis of high-power subcycle field waveforms

E. E. Serebryannikov, V. Ya. Panchenko, and A. M. Zheltikov

Phys. Rev. A **96**, 033853 — Published 28 September 2017

DOI: [10.1103/PhysRevA.96.033853](https://doi.org/10.1103/PhysRevA.96.033853)

Multibeam synthesis of high-power subcycle field waveforms

E. E. Serebryannikov, V. Ya. Panchenko, and A. M. Zheltikov*

Physics Department, International Laser Center, M. V. Lomonosov Moscow State University, Moscow 119992, Russia

Department of Physics and Astronomy, Texas A&M University, College Station TX, 77843-4242 USA and

Russian Quantum Center, ul. Novaya 100, Skolkovo, Moscow Region, 143025 Russia

(Dated: July 7, 2017)

We identify physical scenarios whereby high-peak-power subcycle attosecond field waveforms can be synthesized by coherently combining a multibeam high-order harmonic output generated by a laser driver consisting of a pair of few-cycle pulses with different carrier frequencies. With the relative amplitudes, phases, and group delays of these driver pulses carefully adjusted in each of the driver beams toward confining the recollisions of highest-pondermotive-energy electrons to an extremely short time gate within a fraction of the driver field cycle, the phase-matched multibeam high-harmonic output can be tailored to yield an intense isolated subgigawatt sub-10-attosecond field waveform. As a general tendency, propagation effects are shown to limit the minimum pulse width of the multibeam high-harmonic output. Still, with appropriate optimization of the gas pressure and the beam geometry, ≈ 10 -attosecond field waveforms can be synthesized at the expense of one to two orders of magnitude of the output radiation energy.

PACS numbers: 42.65.Re

I. INTRODUCTION

One of the key challenges confronted by rapidly progressing attosecond technologies [1] is to address the growing demand for the methods and sources for the generation of shorter, more powerful, and better controlled attosecond field waveforms. Within the past few years, ultrafast optical science has benefited tremendously from bright sources of attosecond pulses based on high-order harmonic generation [2–4], as well as from the technology of lightwave synthesizers [5, 6], delivering isolated subcycle, few-femtosecond light pulses in the ultraviolet–visible–near-infrared spectral range. These approaches find growing applications for time-resolved studies and precise manipulation of ultrafast electron dynamics in gases [2, 7–11] and solids [12–15] on the unprecedented time scale.

Field waveform and field cycle engineering methods [16, 17] have been shown to be instrumental in helping address the key challenges in attosecond technologies, allowing high-order harmonics with higher energies and more extended plateaus to be generated, thus opening avenues toward attosecond pulses with shorter pulse widths and higher energies. Optimized field waveforms providing the maximum electron recollision energies have been envisaged by Chipperfield et al. [18] as a way toward enhanced high-order harmonic generation. When implemented in a two-color laser field experiment, this approach provides the increase in the high-harmonic yield by orders of magnitude [19–21] and offers a tool for an attosecond control of electron trajectories in high-harmonic generation [22], promising a technique for the generation of shorter attosecond pulses with a better controlled chirp. In a recent theoretical study [23], two-color fem-

tosecond pulses combined to a sawtooth field waveform have been shown to radically enhance the generation of ultrashort terahertz pulses. A pair of orthogonally polarized ultrashort laser pulses has been demonstrated to provide a powerful tool for steering ultrafast electron dynamics both in time and space, thus giving an access to the fundamental electron processes underlying laser–matter interactions [24–27].

As a route toward attosecond pulses with even shorter pulse width, higher energies, and better controlled field waveforms, we show here that coherent combining of high-harmonic fields generated by a multibeam laser driver consisting of a pair of few-cycle pulses with different carrier frequencies can advantageously integrate the concepts of subcycle pulse synthesizers and high-harmonic attosecond sources into a single multibeam laser scheme, enabling a synthesis of intense subcycle attosecond field waveforms. Our numerical analysis of the time-dependent Schrödinger equation (TDSE) presented below in this paper shows that, with the relative amplitudes, phases, and group delays of the two driver pulses carefully adjusted in each of the driver beams toward confining the recollisions of highest-pondermotive-energy electrons to a minimum time gate within a fraction of the driver field cycle, the multibeam high-harmonic output can be tailored to coherently enhance the flash of harmonics emitted within this extremely short time gate, and to simultaneously suppress, through a destructive interference of high-harmonic beams, the harmonic field outside this time interval. In this regime, intense isolated sub-10-attosecond field waveforms can be synthesized.

II. MULTIBEAM HARMONIC GENERATION

Our approach to a multibeam synthesis of high-power attosecond field waveforms is illustrated in Fig. 1. We

* E-mail to: zheltikov@physics.msu.ru

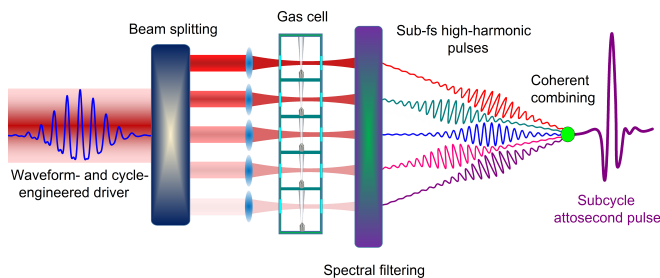


FIG. 1. Multibeam synthesis of high-power subcycle attosecond field waveforms. A carefully waveform- and cycle-engineered high-power laser driver is split into several beams with different intensities to generate high-order harmonics in spatially separated gas jets (shown as a gas cell). High-order harmonic beams are separated from the driver by spatial and spectral filtering and are coherently combined to produce high-intensity attosecond pulses as a result of multibeam interference.

consider a high-power laser driver $E(t) = E_1(t) + E_2(t)$ consisting of two few-cycle optical pulses with different carrier frequencies. The field $E(t)$ is cycle-engineered by varying the relative phase shift $\Delta\phi$, the pulse delay $\Delta\tau$, and the field amplitude ratio E_2/E_1 of the pulses $E_1(t)$ and $E_2(t)$. Analysis presented in this paper was performed for a driver $E(t) = E_1 \cos(\omega t) e^{-(t-\Delta\tau)/\tau_0)^2} + E_2 \cos(2\omega t + \Delta\phi) e^{-(t/\tau_0)^2}$, consisting of a laser pulse with full width at half maximum $\tau_{\text{FWHM}} = \tau_0 \sqrt{2 \ln 2}$ at the fundamental frequency ω_0 and its second harmonic. The laser driver is split into several beams with different intensities, which generate high-order harmonics in spatially separated gas jets [Fig. 1]. High-order harmonic beams generated by such a multibeam two-color laser driver are then separated from the driver by spatial and spectral filtering and are coherently combined to produce high-intensity attosecond pulses as a result of multibeam interference [Fig. 1].

III. SEMICLASSICAL MODEL

To provide insights into the physics enabling attosecond waveform synthesis in the multibeam scheme as outlined above [Fig. 1], we first examine a semiclassical model of high-harmonic generation by a two-color laser driver. In this model, the yield of photoelectrons as a result of field-induced ionization is calculated analytically, by using the Ammosov–Delone–Krainov (ADK) model. The post-ionization dynamics of free electrons driven by the two-color field is then calculated using the Newtonian equations of motion with zero initial velocity and nonzero coordinate $z_0 = I_p/(eE(t))$, to take into consideration a point at which electrons appear in the continuum. Those of free electrons that return to and recollide the nucleus emit optical harmonics [28, 29]. The energy of photons emitted as a part of this harmonic-generation process is

given by $\varepsilon_{ph}(t) = I_p + U_p(t)$ [29], where I_p is the ionization potential and $U_p(t)$ is the pondermotive energy of the recolliding electron at the moment of recollision t , which is calculated through a numerical integration of the classical equation of motion. The energy $\varepsilon_{ph}(t)$ is used in this qualitative treatment as a measure of the maximum harmonic number N_m in the plateau, i.e., the cutoff frequency $\omega_m = N_m \omega_0$, in the spectra of optical harmonics.

In Figs. 2(a)–2(f), we compare semiclassical calculations performed for laser drivers with $\omega_0 = 1.55$ eV (corresponding to an 800-nm output of a Ti: sapphire laser), $\Delta\phi = 0$ [Figs. 2(d), 2(d)] and $\Delta\phi = \pi/2$ [Figs. 2(b), 2(e)] and $\Delta\tau = 0$ [Figs. 2(c), 2(f)] and $T_0/2$ [Figs. 2(a), 2(b), 2(d), 2(e)], $T_0 = 2\pi/\omega_0$ being the driver field cycle. The intensity of the E_1 field in these calculations is set equal to $I_1 = 300$ TW/cm². The pulse widths of both pulses are $\tau_{\text{FWHM}} = 8$ fs, and the amplitude ratio is $E_2/E_1 = 0.3$. The maximum energy $\varepsilon_{ph}(t)$ of photons emitted by electrons moving along these trajectories is shown in Figs. 2(a)–2(c). Classical trajectories of photoelectrons undergoing ionization at different instants of time are presented by blue lines in Figs. 2(d)–2(f). With a spectral filter set to block harmonic radiation with energies below $\varepsilon_f = 70$ eV (corresponding to harmonic numbers $N < 47$), only a few field half-cycles near the center of the laser driver [shown with shading in Figs. 2(a)–2(c)] can generate electrons whose kinetic energies gained by the instant of recollision will be high

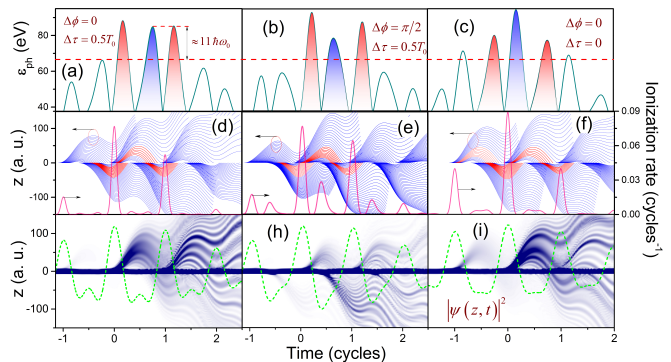


FIG. 2. (a - c) The maximum energy $\varepsilon_{ph}(t)$ of photons emitted by recolliding photoelectrons moving along classical trajectories. The horizontal dotted line shows the edge of the transmission band of the spectral filter, applied to block harmonic radiation with energies below 70 eV. (d - f) Classical trajectories of photoelectrons driven by the two-color laser field (left axis) and the rate of photoionization induced by this field (right axis) as a function of time. (g - i) The maps of the photoelectron probability distribution $|\psi(z, t)|^2$ calculated using the TDSE (shaded blue) and the field of the two-color laser driver (dashed green line). Calculations are performed for a two-color laser driver consisting of a fundamental field with $\omega_0 = 1.55$ eV and its second harmonic, $2\omega_0 = 3.10$ eV, with $I_1 = 300$ TW/cm², $\tau_{\text{FWHM}} = 8$ fs, $E_2/E_1 = 0.3$, $\Delta\phi = 0$ (a, c, d, f) and $\Delta\phi = \pi/2$ (b, e), and $\Delta\tau = 0$ (c, f) and $T_0/2$ (a, b, d, e).

enough to contribute to the harmonic radiation behind the filter. Trajectories of such electrons are shown in red in Figs. 2(d)–2(f). The cycles of the two-color driver thus need to be tailored, through an appropriate choice of $\Delta\phi$, $\Delta\tau$, and E_2/E_1 , in such a way as to suppress harmonics with $\varepsilon_{ph} > 65$ eV from the two field half-cycles adjacent to the central, most intense half-cycle of the driver [red shading in Figs. 2(a)–2(c)]. It is straightforward to see from Figs. 2(a)–2(f) that, with $\Delta\phi = 0$, the two unwanted field half-cycles [blue shading in Figs. 2(a)–2(c)] are strongly suppressed through a destructive interference of $E_1(t)$ and $E_2(t)$. Photoionization is thus drastically reduced, producing no photoelectrons to travel along the trajectories [shown in red in Figs. 2(d)] that could potentially generate high- ε_{ph} harmonics.

Optimization of $\Delta\tau$ and E_2/E_1 , on the other hand, helps maximize the ratio of N_m within the central half-cycle of the field to N_m values in the adjacent half-cycles. In particular, with the time delay set at $\Delta\tau = 0$, photoelectrons produced within the central field half-cycle can generate harmonics with maximum numbers N_m even higher than those attainable with $\Delta\tau = T_0/2$ [cf. Figs. 2(a)–2(c)]. However, the ratios of N_m to the harmonic orders in the adjacent half-cycles of a laser driver with $\Delta\tau = 0$ is noticeably lower than those achieved with $\Delta\tau = T_0/2$ [cf. Figs. 2(a)–2(c)], making a half-cycle delay a much better choice for $\Delta\tau$ in a two-color laser driver. With a suitable choice of the field amplitude ratio E_2/E_1 , as numerical simulations presented below show, the highest contrast of attosecond pulses of harmonic radiation can be achieved.

IV. THREE-DIMENSIONAL TDSE ANALYSIS

For a quantitative analysis, we numerically solve the three-dimensional TDSE for the electron wave function $\psi(r, t)$ with a modified Coulomb potential $V(r) = -\beta(Z/r)\exp(-\gamma r)$ in the presence of a few-cycle two-color laser driver $E(t) = E_1(t) + E_2(t)$. The radiation field reemitted by electrons was calculated as the second-order time derivative of the dipole moment induced by the driver field. The general tendencies in the behavior of the high-harmonic output as a function of the parameters of the two-color laser driver were reliably reproduced in simulations performed for a broad variety of gas targets. For the highest intensities of high-harmonic radiation, however, helium was used as a gas target [$\beta = e^2/(4\pi\epsilon_0)$, $Z = 2$, and $\gamma = 0.707/a_0$, with a_0 being the Bohr radius], allowing higher laser intensities to be applied without saturating ionization [30]. Such a model potential, of course, cannot reproduce all the energy levels of real helium atoms. While many important properties of the optical response of the system may depend on the specific structure of atomic energy levels, attosecond pulses produced by the high-energy part of high-harmonic spectra, considered in this work, are not very sensitive to this factor.

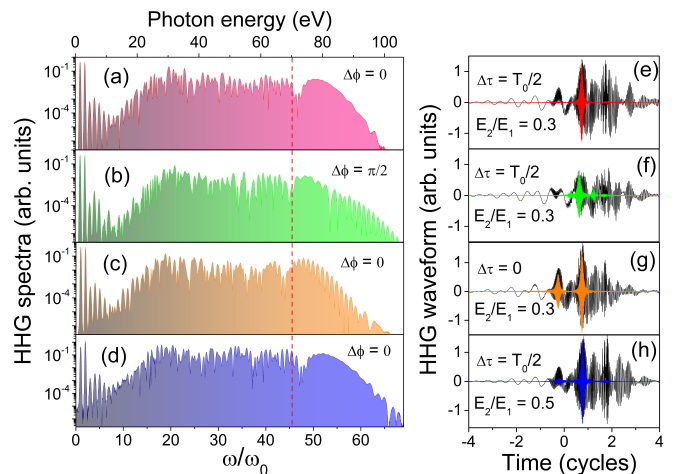


FIG. 3. Spectra (a - d) and field waveforms (e - h) of optical harmonics generated by a two-color laser driver with $\omega_0 = 1.55$ eV, $I_1 = 300$ TW/cm², $\tau_{FWHM} = 8$ fs, $\Delta\phi = 0$ (a, c, d, e, g, h) and $\pi/2$ (b, f), $\Delta\tau = 0$ (c, g) and $T_0/2$ (a, b, d - f, h), and $E_2/E_1 = 0.3$ (a - c, e - f) and 0.5 (d, h). The vertical dashed line shows the edge of the transmission band of the spectral filter, applied to block harmonic radiation with energies below $\varepsilon_f = 70$ eV. The field waveforms of high-harmonic radiation behind this spectral filter are highlighted with color in panels (e - h). The field waveforms of high-harmonic radiation without spectral filtering are shown in black.

The time-domain structure of the high-harmonic field produced by a high-power two-color few-cycle driver is generally quite complicated [Figs. 3(e)–3(h)]. The pulse widths of both fields constituting the two-cycle driver in our scheme, $\tau_{FWHM} = 8$ fs, are long enough to give rise to multiple flashes of high-harmonic emission [Figs. 3(e)–3(h)], representing recolliding photoelectrons driven to their parent ions at different moments of time within the entire duration of the driver. These photoelectron trajectories are visualized in Figs. 2(g)–2(i) by the maps of the photoelectron probability distribution $|\psi(z, t)|^2$, where $|\psi(z, t)|^2 = \int |\psi(z, \rho, t)|^2 d\rho$, ρ being the radial coordinate in the plane orthogonal to z-axis coinciding with laser field polarization. The close resemblance between these maps and classical electron trajectories in Figs. 2(d)–2(f) verifies the predictive power of the semiclassical model, which was used as a guide for driver cycle engineering as explained above.

Results of TDSE simulations [Figs. 3, 4] fully verify predictions of the semiclassical model concerning the regimes enabling the generation of isolated attosecond pulses of high-harmonic radiation. For a two-color laser driver with $I_1 = 300$ TW/cm² and $\tau_{FWHM} = 8$ fs, a single pulse of high-harmonic radiation with a typical pulse width of about 0.25 fs is isolated behind a spectral filter with $\varepsilon_f = 70$ eV (the edge of the transmission band of this filter ε_f is shown by the vertical dashed line in Figs. 3a–3d) when the variables of the laser driver are set at $E_2/E_1 = 0.3$, $\Delta\phi = 0$, and $\Delta\tau = T_0/2$ [Figs. 3(e)–3(h)]. As both semiclassical [Fig. 2d] and TDSE [Fig. 2g]

calculations show, a laser driver with such parameters keeps highest- U_p recolliding electrons, responsible for the highest- ε_{ph} harmonics, tightly confined to a very short time gate within a small fraction of the driver field cycle, yielding extremely short, attosecond isolated flashes of high-harmonic radiation [shown in red in Fig. 3e]. Elsewhere in the parameter space, high- ε_{ph} harmonic generation by the adjacent field half-cycles is not fully suppressed, giving rise to a multipeak structure of high-harmonic emission even behind the spectral filter [shown in color in Figs. 3(f)–3(h)] This result is also in full agreement with semiclassical [Figs. 2(e), 2(f)] and TDSE [Figs. 2(h), 2(i)] calculations.

Two properties of subfemtosecond pulses produced in this scheme of high-harmonic generation are of critical importance for the entire multibeam synthesis concept examined in this work. First, with properly optimized parameters of the driver [$E_2/E_1 = 0.3$, $\Delta\phi = 0$, and $\Delta\tau = T_0/2$ in our case], a subfemtosecond pulse whose phase is flat across its entire spectrum is generated behind the appropriate spectral filter [Fig. 5(a)]. Second, as higher laser intensities translate into higher pondermotive energies U_p of recolliding electrons, the cutoff ε_{ph} in the harmonic spectra is shifted to higher frequencies [Figs. 4(a)–4(c)]. Since the pondermotive energies of recolliding electrons are increased for all the field half-cycles, harmonics of higher orders now need to be filtered to isolate clean single subfemtosecond pulse of high-harmonic radiation [Figs. 4(d)–4(f)]. This is achieved by shifting the transmission edge ε_f of the spectral filter [dashed vertical lines in Figs. 4(a)–4(c)].

Thus, subfemtosecond pulses with a flat phase and tun-

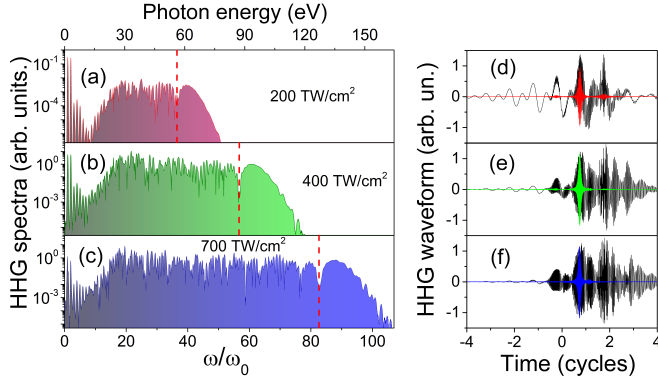


FIG. 4. Spectra (a - c) and field waveforms (d - f) of optical harmonics generated by a two-color laser driver with $\omega_0 = 1.55$ eV, $\tau_{FWHM} = 8$ fs, $\Delta\phi = 0$, $\Delta\tau = T_0/2$, $E_2/E_1 = 0.3$, and $I_1 = 200$ TW/cm² (a, d), 400 TW/cm² (b, e), and 700 TW/cm² (c, f). The vertical dashed line shows the edge of the transmission band of the spectral filter, applied to block harmonic radiation with energies below $\varepsilon_f = 55$ eV (a, d), 87 eV (b, e), and 125 eV (c, f). The field waveforms of high-harmonic radiation behind this spectral filter are highlighted with color in panels (d - f). The field waveforms of high-harmonic radiation without spectral filtering are shown in black.

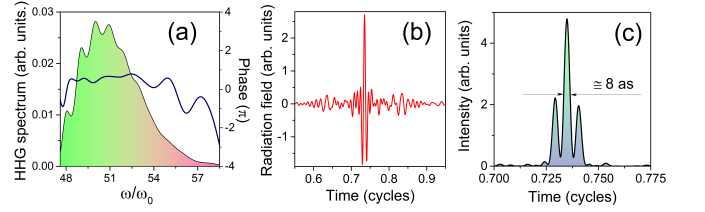


FIG. 5. (a) The spectrum (shading) and the spectral phase (solid line) of the harmonic-radiation pulse generated by a two-color laser driver with $\omega_0 = 1.55$ eV, $I_1 = 300$ TW/cm², $\tau_{FWHM} = 8$ fs, $\Delta\phi = 0$, $\Delta\tau = T_0/2$, and $E_2/E_1 = 0.3$ behind the spectral filter with $\varepsilon_f = 70$ eV. (b, c) The field (b) and intensity (c) waveform of a harmonic-radiation pulse synthesized by coherently combining 11 spectrally filtered high-harmonic beams generated by an 11-beam two-color laser driver with $I_1 = 200$ TW/cm², $\Delta = 100$ TW/cm², $\tau_{FWHM} = 8$ fs, $\Delta\phi = 0$, $\Delta\tau = T_0/2$, and $E_2/E_1 = 0.3$

able spectra can be generated by using a two-color laser driver with properly optimized parameters and a variable field intensity. This suggests that, with the laser driver split into M beams with intensities in the E_1 beam $I_j = I_1 + (j-1)\Delta$, where $j = 1, \dots, M$ and Δ is the increment in intensity from one beam to another, an extremely short isolated pulse of high-harmonic radiation can be synthesized by coherently combining the high-harmonic outputs produced by individual beams of the laser driver in M spatially separated gas jets [Fig. 1].

Such a coherent combining of high-harmonic outputs generated by an M -beam two-color driver is illustrated in Figs. 4, 5(b), 5(c). In this example, we take $\omega_0 = 1.55$ eV, $I_1 = 200$ TW/cm², $\Delta = 100$ TW/cm², and $M = 11$ with $\tau_{FWHM} = 8$ fs, $\Delta\phi = 0$, $\Delta\tau = T_0/2$, and $E_2/E_1 = 0.3$ in each of the 11 beams. With a spectral filter set to reject the low-frequency part of the spectrum [as shown in Figs. 4(a)–4(c)], viz., harmonics with $N < 36, 47, 56, 65, 75, 83, 90, 97, 103, 109, 115$, for $j = 1, \dots, 11$, high-harmonic pulses with a pulse width of 0.2 – 0.3 fs [Figs. 4(d)–4(f)] are produced behind the respective spectral filters in each of the 11 beams. Coherent addition of these 11 high-harmonic pulses without any additional phase compensation (which may still be needed to correct for inevitable variations in the parameters of the gas jets and individual beam geometries) yields an ultrashort field waveform [Figs. 5(b), 5(c)] with a pulse width, defined as the full width at half-maximum of the field intensity profile [Fig. 5(c)], as short as 8 attoseconds.

With a typical beam waist diameter in a gas jet set at $d \approx 35$ μm , the overall laser energy needed to deliver an ultrashort-pulse multibeam driver with $I_1 = 200$ TW/cm², $\Delta = 100$ TW/cm², and $M = 11$ is about 0.5 mJ. With an upper-bound estimate of 10^{-5} for the efficiency of harmonic generation in the considered spectral range [31], multibeam harmonic generation implemented with submillijoule laser drivers can be expected to yield sub-10-attosecond high-harmonic waveforms, as shown in

Figs. 5(b) and 5(c), with a peak power within the central peak of about 0.5 GW. Even shorter, subattosecond pulses with tailored waveforms can be generated through a finer multibeam driver optimization within the class of driver fields comprising more than two laser pulses, fields with incommensurate frequencies, or carefully chirped supercontinua. Generation of subattosecond field waveforms with peak powers of several gigawatts can be anticipated for multibeam synthesis schemes with a larger number of laser beams in experiments that could be implemented using the available 100-TW-class laser sources.

V. MACROSCOPIC TREATMENT

The full analysis of the macroscopic high-harmonic response of a gas medium to an ultrashort laser driver has to include field-evolution effects [32, 33], which tend to distort ultrashort field waveforms synthesized as a part of high-harmonic generation [34]. To include these effects into our model, we solve the field evolution equations for the laser driver and high-harmonic fields E_l and E_h

$$\frac{\partial E_l(\zeta, r, \omega)}{\partial \zeta} = i \left(k(\omega) - \frac{\omega}{u} \right) E_l(\zeta, r, \omega) + i \frac{1}{2k(\omega)} \nabla_{\perp}^2 E_l(\zeta, r, \omega) + i \frac{\mu_o \omega^2}{2k(\omega)} P_{nl}(\zeta, r, \omega) - i \frac{\mu_o}{2k(\omega)} \frac{e^2}{m_e} \hat{F} \left\{ \tilde{E}_l n_e \right\} \quad (1)$$

$$\frac{\partial E_h(\zeta, r, \Omega)}{\partial \zeta} = i \left(k(\Omega) - \frac{\Omega}{u} + i\alpha(\Omega) \right) E_h(\zeta, r, \Omega) + i \frac{1}{2k(\Omega)} \nabla_{\perp}^2 E_h(\zeta, r, \Omega) + i \frac{\mu_o \Omega^2}{2k(\Omega)} P_{nl}(\zeta, r, \Omega) \quad (2)$$

where $\tilde{E}_l(\zeta, r, t)$ is the laser driver field, $E_l(\zeta, r, \omega)$ is its Fourier transform, ζ is the propagation coordinate, r is the radial coordinate, $E_h(\zeta, r, \Omega)$ is the harmonic field, u is the driver field group velocity, $k(\omega') = \omega' n_i(\omega')/c$, $\omega' = \omega$ for the laser driver and $\omega' = \Omega$ for the high-harmonic field, $n_i(\omega')$ is the refractive index, c is the speed of light in vacuum, $\alpha(\Omega)$ is the absorption coefficient, $\hat{F}\{\}$ is the Fourier transform operator, $n_e(\zeta, r, t)$ is the electron density, $P_{nl}(\zeta, r, \omega')$ is the Fourier transform of the nonlinear polarization, m_e and e are the electron mass and charge, respectively. The field-evolution equations (1) and (2) are solved jointly with the equation for the electron density $n_e(\zeta, r, t)$,

$$\frac{\partial n_e(\zeta, r, t)}{\partial t} = W(\zeta, r, t) [n_A(z) - n_e(z, r, t)] \quad (3)$$

where $W(\zeta, r, t)$ is the ionization rate and $n_A(\zeta)$ is the density of neutral species interacting with the laser field.

We apply these equations to examine multibeam waveform synthesis using high-order harmonic generation in a helium jet. Due to its high ionization potential ($U_{ion} \approx 24.6$ eV), helium helps avoid ionization saturation within the considered range of driver field intensities. Dispersion and absorption spectra of helium were included in the model in accordance with the standard reference data [35, 36]. The spatial profile of neutral-gas density in a gas jet [Fig. 6(a)] is modeled as $n_A(\zeta) = p \exp(-((\zeta - \zeta_0)/\Delta\zeta)^6)/(k_B T)$, where p is the gas pressure at the center of the jet $\zeta = \zeta_0$, $\Delta\zeta$ is the width of the gas jet, T is the gas temperature in the jet, and k_B is the Boltzmann constant.

The nonlinear polarization giving rise to high-order harmonic generation is written as $P_{nl}(\zeta, r, \Omega) = n_A(\zeta) d(r, \Omega)$, with the dipole moment $d(r, \Omega)$ calculated

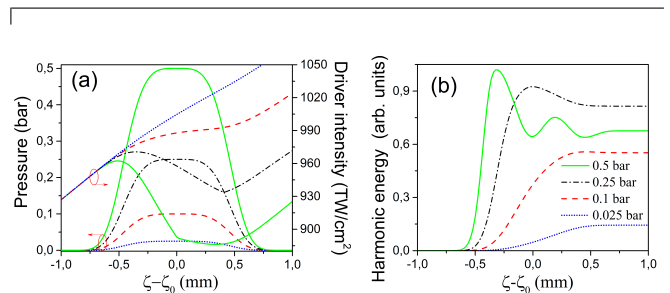


FIG. 6. The peak intensity of the driver (a) and the high-harmonic output energy (b) as a function of the propagation coordinate for a two-color driver with integral energy equal 0.25 mJ, $E_2/E_1 = 0.3$, $\Delta\tau = T_0/2$, $\Delta\phi = 0$ propagating through a helium jet with a pressure profile shown at panel (a) with $p = 0.025$ bar (dotted blue line), 0.1 bar (dashed red line), 0.25 bar (dash-dotted black line), and 0.5 bar (solid green line). The gas jet is centered at $\zeta_0 = 0.497$ m.

within the framework of strong-field approximation (see, e.g., Ref. [37]). The laser driver field is taken in the form of an ultrashort two-color pulse with parameters as specified above (dashdotted line in Fig. 7(a)). The ionization rate W in (3) is calculated using the Yudin–Ivanov formula [38].

Unless special measures are taken toward optimizing the gas pressure and beam geometry, phase and group-velocity mismatch, the Gouy phase shift, ionization-induced absorption and spatial self-action of the driver [Fig. 6(a)] strongly influence high-order harmonic generation [Fig. 6(b)], heavily distorting the field waveform emitted as a result of high-order harmonic generation. Specifically, for gas pressures, roughly, above 0.1 bar, these effects are prohibitively strong, leaving no parameter space for attosecond pulse generation as a result of

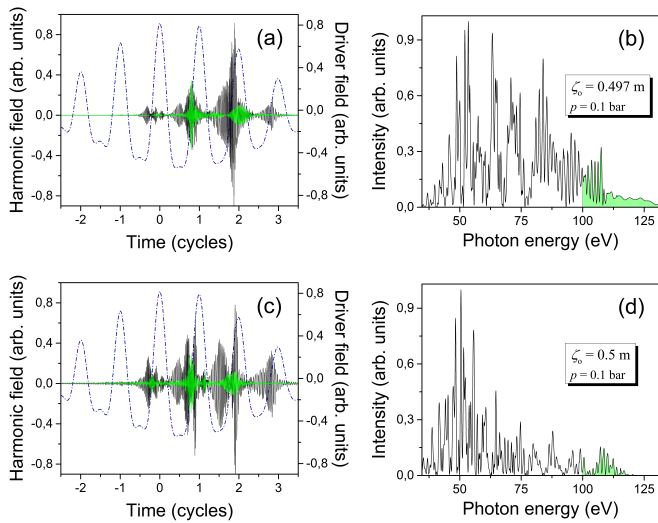


FIG. 7. The waveforms (a, c) and the spectra (b, d) of the high-harmonic field generated by a two-color ultrashort driver (dashdotted line) with field intensity $I = 1000 \text{ TW/cm}^2$ in a helium jet with $p = 0.10 \text{ bar}$ (a, b) and 0.25 bar (c, d). The green line shows the high-harmonic field corresponding to the highest-frequency part of the harmonic spectrum (shown by green shading). The beam waist is located at $f = 0.5 \text{ m}$. The gas jet is centered at $\zeta_0 = 0.497 \text{ m}$ (a, b) and 0.5 m (c, d).

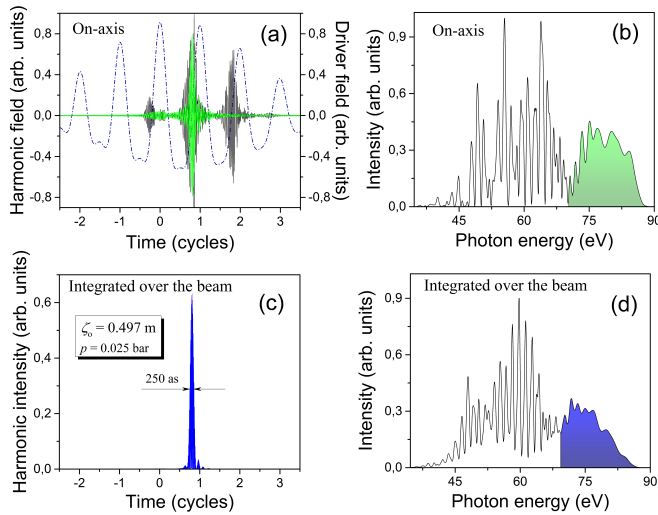


FIG. 8. The on-axis waveform (a) and the on-axis spectrum (b) of the high-harmonic field generated by a two-color ultrashort driver (dashdotted line) with field peak intensity $I = 500 \text{ TW/cm}^2$ in a helium jet with $p = 25 \text{ mbar}$. The green line shows the high-harmonic field corresponding to the highest-frequency part of the harmonic spectrum (shown by green shading). (c) The waveform of the spectrally filtered high-harmonic field integrated over the entire beam. (d) The spectrum of the high-harmonic field integrated over the entire beam. The high-frequency part of the spectrum corresponding to the attosecond pulse in panel (c) is shown by blue shading. The beam waist is located at $f = 0.5 \text{ m}$. The gas jet is centered at $\zeta_0 = 0.497 \text{ m}$.

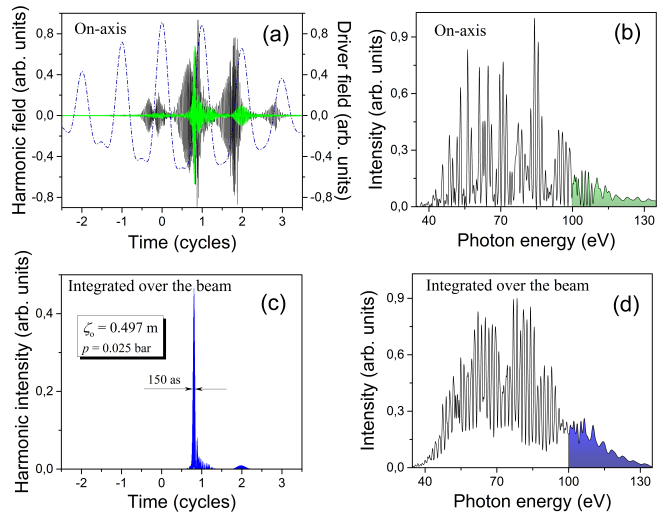


FIG. 9. The on-axis waveform (a) and the on-axis spectrum (b) of the high-harmonic field generated by a two-color ultrashort driver (dashdotted line) with field peak intensity $I = 1000 \text{ TW/cm}^2$ in a helium jet with $p = 25 \text{ mbar}$. The green line shows the high-harmonic field corresponding to the highest-frequency part of the harmonic spectrum (shown by green shading). (c) The waveform of the spectrally filtered high-harmonic field integrated over the entire beam. (d) The spectrum of the high-harmonic field integrated over the entire beam. The high-frequency part of the spectrum corresponding to the attosecond pulse in panel (c) is shown by blue shading. The beam waist is located at $f = 0.5 \text{ m}$. The gas jet is centered at $\zeta_0 = 0.497 \text{ m}$.

multibeam high-order harmonic generation [Figs. 7(a), 7(b)].

As the gas pressure in the jet is lowered to approximately 0.1 bar , propagation-induced distortions become weaker. In this regime, reasonably broad, continuous bands start to show up in the high-frequency wings of high-harmonic spectra [Fig. 7(a)], exposing the properties of high-order harmonics as described in Section IV and illustrated in Figs. 3 and 4. At gas pressures below 0.1 bar , attosecond high-harmonic waveforms can be generated with a careful optimization of the driver beam waist relative to the gas jet. As two typical examples, Figures 8 and 9 show that, with the driver beam waist positioned 3 mm behind the center of the gas jet, where the gas pressure is set at $p = 25 \text{ mbar}$, high-harmonic pulses as short as $0.15 - 0.25 \text{ fs}$ can be produced through appropriate spectral filtering. Moreover, the spectrum of the attosecond high-harmonic output can be tuned, as shown in Figs. 8 and 9, by varying the intensity of the laser driver. In a scheme of multibeam harmonic generation (Fig. 1) with $M = 11$, this enables a synthesis of pulses as short as approximately 10 attoseconds . The energy of these pulses is, however, one to two orders of magnitude lower than the energy of sub-10-attosecond pulses attainable in the regime of perfect phase matching (Section IV).

VI. CONCLUSION

To summarize, we have identified physical scenarios whereby subcycle attosecond field waveforms can be synthesized by coherently combining a multibeam high-order harmonic output generated by a laser driver consisting of a pair of few-cycle pulses with different carrier frequencies. With the relative amplitudes, phases, and group delays of these driver pulses carefully adjusted in each of the driver beams toward confining the recollisions of highest-pondermotive-energy electrons to an extremely short time gate within a fraction of the driver field cycle, the multibeam high-harmonic output can be tailored to yield intense isolated subgigawatt sub-10-attosecond field waveforms. As a general tendency, phase and group-velocity mismatch, the Gouy phase shift, ionization-

induced absorption and spatial self-action of the driver are shown to limit the minimum pulse width of the multibeam high-harmonic output. Still, with appropriate optimization of the gas pressure and the beam geometry, ≈ 10 -attosecond field waveforms can be synthesized at the expense of one to two orders of magnitude of the output radiation energy.

ACKNOWLEDGMENTS

This research was supported in part by the Russian Foundation for Basic Research (project nos. 14-29-07182, 16-29-11789 and 16-02-00843), the Welch Foundation (Grant No. A-1801), and ONR (Award No. 00014-16-1-2578). Research into the nonlinear optics in the mid-infrared has been supported by the Russian Science Foundation (project no. 14-12-00772).

-
- [1] P. B. Corkum and F. Krausz, *Nature Phys.* **3**, 381 (2007).
 [2] M. Hentschel, R. Kienberger, C. Spielmann, G. A. Reider, N. Milosevic, T. Brabec, P. Corkum, U. Heinzmann, M. Drescher, and F. Krausz, *Nature* **414**, 509 (2001).
 [3] E. Goulielmakis, V. S. Yakovlev, A. L. Cavalieri, M. Uiberacker, V. Pervak, A. Apolonski, R. Kienberger, U. Kleineberg, and F. Krausz, *Science* **317**, 769 (2007).
 [4] E. Goulielmakis, M. Schultze, M. Hofstetter, V. S. Yakovlev, J. Gagnon, M. Uiberacker, A. L. Aquila, E. M. Gullikson, D. T. Attwood, R. Kienberger, F. Krausz, and U. Kleineberg, *Science* **320**, 1614 (2008).
 [5] A. Wirth, M. T. Hassan, I. Grguraš, J. Gagnon, A. Moulet, T. T. Luu, S. Pabst, R. Santra, Z. A. Alahmed, A. M. Azzeer, V. S. Yakovlev, V. Pervak, F. Krausz, and E. Goulielmakis, *Science* **334**, 195 (2011).
 [6] S.-W. Huang, G. Cirmi, J. Moses, K.-H. Hong, S. Bhardwaj, J. R. Birge, L.-J. Chen, E. Li, B. J. Eggleton, G. Cerullo, and F. X. Kartner, *Nat. Photon.* **5**, 475 (2011).
 [7] J. Itatani, J. Levesque, D. Zeidler, H. Niikura, H. Pepin, J. C. Kieffer, P. B. Corkum, and D. M. Villeneuve, *Nature* **432**, 867 (2004).
 [8] H. Akagi, T. Otobe, A. Staudte, A. Shiner, F. Turner, R. Dörner, D. M. Villeneuve, and P. B. Corkum, *Science* **325**, 1364 (2009).
 [9] A. N. Pfeiffer, C. Cirelli, M. Smolarski, D. Dimitrovski, M. Abu-samha, L. B. Madsen, and U. Keller, *Nature Phys.* **8**, 76 (2012).
 [10] D. Shafir, H. Soifer, B. D. Bruner, M. Dagan, Y. Mairesse, S. Patchkovskii, M. Y. Ivanov, O. Smirnova, and N. Dudovich, *Nature* **485**, 343 (2012).
 [11] M. T. Hassan, T. T. Luu, A. Moulet, O. Raskazovskaya, P. Zhokhov, M. Garg, N. Karpowicz, A. M. Zheltikov, V. Pervak, F. Krausz, and E. Goulielmakis, *Nature* **530**, 66 (2016).
 [12] S. Neppl, R. Ernstorfer, A. L. Cavalieri, C. Lemell, G. Wachter, E. Magerl, E. M. Bothschafter, M. Jobst, M. Hofstetter, U. Kleineberg, J. V. Barth, D. Menzel, J. Burgdorfer, P. Feulner, F. Krausz, and R. Kienberger, *Nature* **517**, 342 (2015).
 [13] M. Schultze, M. Fieß, N. Karpowicz, J. Gagnon, M. Korbman, M. Hofstetter, S. Neppl, A. L. Cavalieri, Y. Komninos, T. Mercouris, C. A. Nicolaides, R. Pazourek, S. Nagele, J. Feist, J. Burgdörfer, A. M. Azzeer, R. Ernstorfer, R. Kienberger, U. Kleineberg, E. Goulielmakis, F. Krausz, and V. S. Yakovlev, *Science* **328**, 1658 (2010).
 [14] F. Krausz and M. I. Stockman, *Nat. Photon.* **8**, 205 (2014).
 [15] T. T. Luu, M. Garg, S. Y. Kruchinin, A. Moulet, M. T. Hassan, and E. Goulielmakis, *Nature* **521**, 498 (2015).
 [16] J. Mauritsson, P. Johnsson, E. Gustafsson, A. L'Huillier, K. J. Schafer, and M. B. Gaarde, *Phys. Rev. Lett.* **97**, 013001 (2006).
 [17] S. B. P. Radnor, L. E. Chipperfield, P. Kinsler, and G. H. C. New, *Phys. Rev. A* **77**, 033806 (2008).
 [18] L. E. Chipperfield, J. S. Robinson, J. W. G. Tisch, and J. P. Marangos, *Phys. Rev. Lett.* **102**, 063003 (2009).
 [19] F. Calegari, C. Vozzi, M. Negro, G. Sansone, F. Frassetto, L. Poletto, P. Villoresi, M. Nisoli, S. D. Silvestri, and S. Stagira, *Opt. Lett.* **34**, 3125 (2009).
 [20] T. Siegel, R. Torres, D. J. Hoffmann, L. Brugnera, I. Prochino, A. Zaïr, J. G. Underwood, E. Springate, I. C. E. Turcu, L. E. Chipperfield, and J. P. Marangos, *Opt. Express* **18**, 6853 (2010).
 [21] L. Brugnera, F. Frank, D. J. Hoffmann, R. Torres, T. Siegel, J. G. Underwood, E. Springate, C. Froud, E. I. C. Turcu, J. W. G. Tisch, and J. P. Marangos, *Opt. Lett.* **35**, 3994 (2010).
 [22] M. Fieß, B. Horvath, T. Wittmann, W. Helml, Y. Cheng, B. Zeng, Z. Xu, A. Scrinzi, J. Gagnon, F. Krausz, and R. Kienberger, *New J. Phys.* **13**, 033031 (2011).
 [23] P. G. d. A. Martínez, I. Babushkin, L. Bergé, S. Skupin, E. Cabrera-Granado, C. Köhler, U. Morgner, A. Husakou, and J. Herrmann, *Phys. Rev. Lett.* **114**, 183901 (2015).
 [24] L. Zhang, X. Xie, S. Roither, D. Kartashov, Y. Wang, C. Wang, M. Schöffler, D. Shafir, P. B. Corkum, A. Baltuška, I. Ivanov, A. Kheifets, X. Liu, A. Staudte, and M. Kitzler, *Phys. Rev. A* **90**, 061401 (2014).

- [25] M. Richter, M. Kunitski, M. Schöffler, T. Jahnke, L. P. H. Schmidt, M. Li, Y. Liu, and R. Dörner, *Phys. Rev. Lett.* **114**, 143001 (2015).
- [26] L. Zhang, X. Xie, S. Roither, Y. Zhou, P. Lu, D. Kartashov, M. Schöffler, D. Shafir, P. B. Corkum, A. Baltuška, A. Staudte, and M. Kitzler, *Phys. Rev. Lett.* **112**, 193002 (2014).
- [27] J.-W. Geng, W.-H. Xiong, X.-R. Xiao, L.-Y. Peng, and Q. Gong, *Phys. Rev. Lett.* **115**, 193001 (2015).
- [28] P. B. Corkum, *Phys. Rev. Lett.* **71**, 1994 (1993).
- [29] M. Lewenstein, P. Balcou, M. Y. Ivanov, A. L’Huillier, and P. B. Corkum, *Phys. Rev. A* **49**, 2117 (1994).
- [30] T. Popmintchev, M.-C. Chen, D. Popmintchev, P. Arpin, S. Brown, S. Ališauskas, G. Andriukaitis, T. Balčiunas, O. D. Mücke, A. Pugžlys, A. Baltuška, B. Shim, S. E. Schrauth, A. Gaeta, C. Hernández-García, L. Plaja, A. Becker, A. Jaron-Becker, M. M. Murnane, and H. C. Kapteyn, *Science* **336**, 1287 (2012).
- [31] E. Constant, D. Garzella, P. Breger, E. Mével, C. Dorrer, C. Le Blanc, F. Salin, and P. Agostini, *Phys. Rev. Lett.* **82**, 1668 (1999).
- [32] A. B. Fedotov, S. M. Gladkov, N. I. Koroteev, and A. M. Zheltikov, *J. Opt. Soc. Am. B* **8**, 363 (1991).
- [33] T. Popmintchev, M.-C. Chen, A. Bahabad, M. Gerrity, P. Sidorenko, O. Cohen, I. P. Christov, M. M. Murnane, and H. C. Kapteyn, *Proc. Nat. Acad. Sci.* **106**, 10516 (2009).
- [34] A. Moulet, V. Tosa, and E. Gouilelmakis, *Opt. Lett.* **39**, 6189 (1991).
- [35] C. R. Mansfield and E. R. Peck, *J. Opt. Soc. Am.* **59**, 199 (1969).
- [36] http://henke.lbl.gov/optical_constants/.
- [37] V. S. Yakovlev, M. Ivanov, and F. Krausz, *Opt. Express* **15**, 15351 (2007).
- [38] G. L. Yudin and M. Y. Ivanov, *Phys. Rev. A* **64**, 013409 (2001).